Research Article Vol. 10, No. 10 / October 2023 / Optica 1383

OPTICA

Noncollinear, inelastic four-wave mixing in the extreme ultraviolet

R. Mincigrucci,[1,*] A. Cannizzo,[2] F. Capotondi,[1] P. Cinquegrana,[1] R. Cucini,[3] F. Dallari,[4] M. B. Danailov,[1] G. De Ninno,[1,5] S. Di Mitri,[1] T. Feurer,[2] L. Foglia,[1] H.-M. Frei,[2] M. Manfredda,[1] A. A. Maznev,[6] G. Monaco,[4] D. Naumenko,[1] I. Nikolov,[1] Z. Ollmann,[2] E. Paltanin,[1] G. Pamfilidis,[2] E. Pedersoli,[1] E. Principi,[1] J. Rehault,[3] A. Simoncig,[1] C. Svetina,[7] G. Knopp,[8] C. Masciovecchio,[1] and F. Bencivenga[1]

[1]Elettra-Sincrotrone Trieste S.C.p.A., S.S. 14 km 163,5 in Area Science Park, I-34012 Basovizza, Trieste, Italy
[2]Institute of Applied Physics, University of Bern, Sidlerstrasse 5, CH-3012, Bern, Switzerland
[3]CNR-IOM, Strada Statale 14, km 163.5, Trieste, Italy
[4]Dipartimento di Fisica e Astronomia "Galileo Galilei", Università degli Studi di Padova, 35131 Padova, Italy
[5]Laboratory of Quantum Optics, University of Nova Gorica, 5001 Nova Gorica, Slovenia
[6]Massachusetts Institute of Technology, 77 Massachusetts Avenue, Cambridge, Massachusetts 02139, USA
[7]IMDEA Nanociencia, Faraday 9, 28049 Madrid, Spain
[8]Paul Scherrer Institute, CH-5232 Villigen, Switzerland
*riccardo.mincigrucci@elettra.eu

Received 14 June 2023; revised 18 September 2023; accepted 18 September 2023; published 16 October 2023

Driving four-wave mixing (FWM) processes with extreme ultraviolet (EUV) pulses could enable experimental approaches that have the potential to provide unique information on dynamics and correlations. In this work, we demonstrate inelastic FWM obtained by noncollinear mixing of two EUV pulses with different photon energies and an optical pulse in a diamond sample. This three-pulse interaction leads to the emission of an optical signal, propagating in the phase-matching direction and blue shifted by the photon energy difference of the two EUV pulses. The presented results demonstrate the feasibility of experiments such as the soft X-ray analogue of coherent anti-Stokes Raman scattering, so far only theoretically conceived [Phys. Rev. Lett. 89, 043001 (2002)], which can be further extended for studying vibrational and electronics dephasing in solid, liquid, or gaseous samples.

https://doi.org/10.1364/OPTICA.497745

1. INTRODUCTION

Nonlinear optics (NLO) techniques arise from the simultaneous interaction of two or more (input) light fields with a sample, which drive the emission of a (output) "signal field." NLO methods have been thoroughly used in the optical regime to study dynamics and correlations inaccessible by linear methods, as well as to greatly improve selectivity and sensitivity of optical measurements [1]. The list of applications of NLO can easily be longer than the present paper, as they range from sunlight harvesting [2] to photonics [3], quantum communications [4], magnetism [5], heat transport [6], and biology [7].

The use of multiple light fields to interrogate the sample permits to conceive the so-called noncollinear experimental geometries where, because of energy and momentum conservation, the signal fields are emitted into "background free directions," i.e., directions vastly different from those of the input fields. Noncollinear set-ups, where the pulses cross at an angle θ at the sample, are often more complex but reward the experimentalists with a high signal-to-noise ratio (S/N). However, NLO methods based on optical lasers are inherently limited by the relatively small wavevector (k) and low photon energy (E) of optical photons. In most practical cases, this precludes obtaining information on atomic and molecular scale structures and excitations, as well as using atom-specific transitions to achieve elemental and chemical selectivity. These limitations can be overcome and new breakthroughs enabled by extending NLO into the x-ray regime, as has been proposed on theoretical grounds [8–10]. Despite the rich theoretical literature, the experiments had to wait until the rise of free electron lasers (FELs) and high harmonic generation (HHG) sources, which enabled the experimentalists to exploit intense and ultrafast pulses in the extreme ultraviolet (EUV) and x-ray spectral regions.

Some key studies have been already conducted [11–16], among them an EUV-optical experiment where a third-order nonlinear process [four-wave mixing (FWM)] involving two optical photons and an EUV photon with photon energy tuned at a specific core resonance ($E_{EUV} \approx 62$ eV; Li K-edge) was used to assess the electron and hole co-localization [17]. This fundamental study was performed in a collinear geometry and demonstrated the possibility to generate and detect an EUV-optical "inelastic" FWM signal, i.e., with a photon energy ($E_{sig} = E_{EUV} \pm 2E_{opt}$) equal neither to

E_{EUV} nor to the optical photon energy E_{opt}. Such a "combined" EUV-optical inelastic FWM signal encoded information that would not have been accessible by single-photon (either only EUV or only optical) interactions.

In the present work, we report on a noncollinear EUV-optical FWM process, where two EUV photons with different photon energies (E_{EUV1} and E_{EUV2}) and an optical photon generate a noncollinear inelastic FWM signal at $E_I = E_{opt} + \Delta E$, with $\Delta E = E_{EUV2} - E_{EUV1}$, whose emission direction is determined by energy and momentum conservation. The excitation mechanism can be depicted as a grating moving in time during the illumination with a velocity of $\frac{\Delta E}{\hbar}|\boldsymbol{k}|^{-1}$ along the direction $\boldsymbol{k} = \boldsymbol{k}_{EUV2} - \boldsymbol{k}_{EUV1}$; see Supplement 1.

The noncollinear approach used in our work allowed for a better S/N with respect to collinear approaches, which permitted observing the FWM signal even in the absence of any EUV absorption resonance, namely, in a situation where EUV-optical FWM signals are expected to be smaller by orders of magnitude [1,18] compared to resonant FWM; note that in Ref. [17], no signal was observed out of the EUV resonance. The employed set-up also has the advantage of allowing the study of the FWM response as a function of both relative delays among the three input pulses.

Another intrinsic advantage of the noncollinear approach is represented by the possibility to vary the crossing angle between the EUV pulses ($2\theta_{FF}$) to change the EUV "grating vector" $|\boldsymbol{k}|$ while keeping ΔE fixed. For example, independently scanning $|\boldsymbol{k}|$ and exploiting EUV core–hole resonances could permit to extract spatial information about the sites where such core–holes are located [8,19,20].

2. MATERIALS AND METHODS

Figure 1(a) shows a sketch of the experiment, which is based on the mini-TIMER set-up [21], used for noncollinear EUV-optical transient grating (TG) experiments and on the twin-seed operation mode of the FERMI FEL [22]. The latter was used to generate a sequence of two EUV pulses, separated in time by ≈ 350 fs, the first one with $E_{EUV1} = 47.7$ eV and the second one with $E_{EUV2} = 47.88$ eV; E_{EUV2} can be varied from 47.7 to ≈ 48.2 eV. The two pulses have an estimated time duration of ≈ 50 fs [full width at half maximum (FWHM)] and are separated in time by about 350 fs [22]; both of them are linearly polarized, orthogonally to the plane of the drawing in Fig. 1(a).

The main limitation of this set-up is represented by the impossibility to prevent pre- and post- pulses [labeled as E^B_{EUV1} and E^A_{EUV2} in Fig. 1(a)] from reaching the sample. The presence of the pre-pulse rules out the investigation of ground-state phenomena, while the post-pulse inherently complicates the investigation of dynamics. However, for the demonstrative purpose of the present work, this set-up has the essential advantage of being simple and robust. Some technically feasible alternatives to overcome this limitation will be discussed in the conclusion.

The energy per pulse and spot size at the sample were, respectively, 8 μJ and 150 × 200 μm^2 (horizontal × vertical; FWHM), resulting in a fluence of 20 mJ/cm^2. The split and recombination were achieved by the mini-timer set-up and resulted in two beams, labeled with the suffixes A and B in Fig. 1(a), each one consisting of the aforementioned sequence of two FEL pulses. These two beams were recombined at the sample with a semi-angle $\theta_{FF} = 2.7°$. The optical probe beam with $E_{opt} = 3.16$ eV impinged onto the sample at an angle $\theta_{FL} = 45°$, and its pulse energy, spot size, and

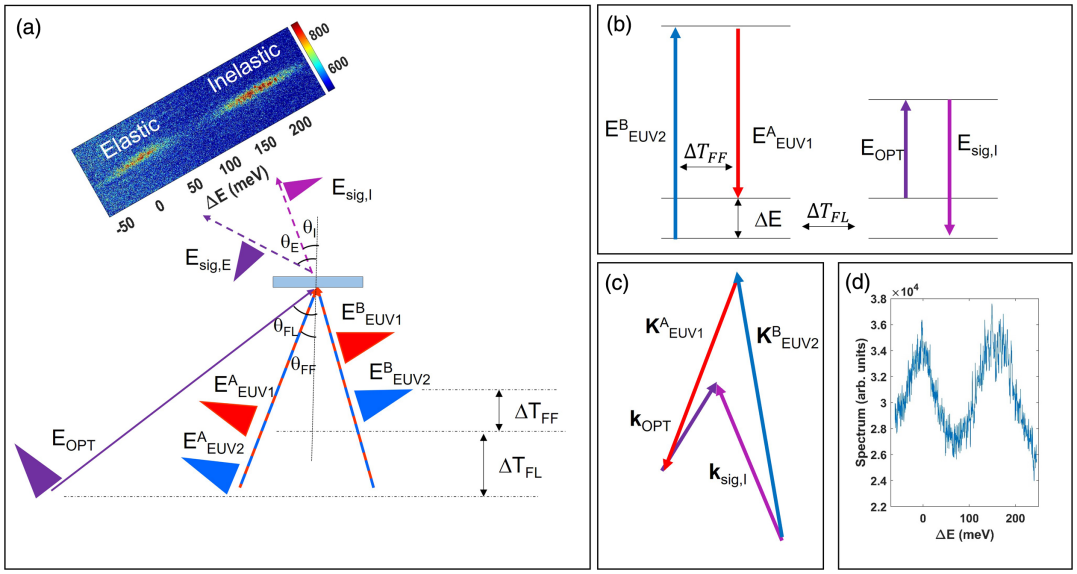

Fig. 1. (a) Sketch of the experiment. Two sequences (labeled by suffixes "A" and "B") of FEL pulses with $E_{EUV1} = 47.70$ eV and $E_{EUV2} = 47.88$ eV are recombined at the sample position with a semi-angle $\theta_{FF} = 2.7°$. The optical probe beam with $E_{opt} = 3.16$ eV impinges at the FEL crossing point with an angle $\theta_{FL} = 45°$. In addition to the expected inelastic FWM emitted at $\theta_I = 42.8°$ ($E_{sig,I} = 3.34$ eV), we observed an additional "elastic" signal emitted at $\theta_E = 45.6°$ ($E_{sig,E} = 3.16$ eV). All the angles are measured with respect to the sample normal. A high pass filter with a transmission ratio of ∼40 in favor of the inelastic signal, not shown in the figure, was placed in front of the detector. ΔT_{FF} is the time delay between FEL pulse sequences "A" and "B," while ΔT_{FL} is the time delay between the laser pulse and the FEL pulse labeled as E^A_{EUV2}; see text for further details. The two elongated spots in the image are the inelastic and elastic FWM signals, respectively emitted at θ_I and θ_E, as collected by the CCD detector at $(\Delta T_{FF}, \Delta T_{FL}) = (0, 0)$. (b) Energy conservation diagram for the process that generates the inelastic signal. When $(\Delta T_{FF}, \Delta T_{FL}) = (0, 0)$, the two FEL pulses ($E^A_{EUV2}$, E^B_{EUV1}) force a nonlinear polarization oscillating at $\Delta E/\hbar$, which couples with the probe field (oscillating at $E_{OPT}/\hbar$), driving the emission of a FWM signal beam at $E_{opt} + \Delta E$. The length of the arrows does not reflect the relative values of the photon energies. (c) Corresponding momentum conservation diagram; the length of the arrows does not reflect the magnitude of the wavevectors. See Supplement 1. (d) Spectrum of the signal reported in the inset of (a).

time duration were, respectively, 2.5 μJ, 200 × 200 μm FWHM, and ≈ 100 fs FWHM. The probe beam was linearly polarized, orthogonally to the panel of Fig. 1(a). The sample was a 5 mm thick, chemical vapor deposited diamond crystal with the surface exposed to the FEL beam corresponding to the [100] crystallographic plane. Diamond was chosen for its high nonlinear response [23,24] and radiation resistance [25].

The inelastic FWM signal beam has an expected photon energy $E_{\mathrm{sig},I} = E_{\mathrm{opt}} + \Delta E$, as shown in the energy level diagram shown in Fig. 1(b), and is expected to be emitted along a "background-free" direction, since the emission angle (θ) was very different from all incidence angles; see Fig. 1(a) and momentum conservation diagram in Fig. 1(c). The geometry of the experiment was conceived to collect the signal both when $\Delta E = 0$ and when $\Delta E > 0$, up to $\Delta E \approx 300$ meV, using a position-sensitive detector (PI-MTE camera).

It is possible to calculate the values of θ, which were $\theta_I = 42.8°$ for $\Delta E = 180$ meV and $\theta_E = 45.6°$ for $\Delta E = 0$. Therefore, the determination of θ straightforwardly acts as a spectral analysis of the signal. To further increase the S/N, a high pass optical filter (FGUV11 by Thorlabs) was placed in front of the detector to remove residual light leaking into the experimental chamber and reduce diffuse light at E_{opt}. In fact, the filter transmission at E_{opt} was 1% while it was 43% at $E_{\mathrm{sig},I} = E_{\mathrm{opt}} + \Delta E$, where $\Delta E = 180$ meV is the value used in the present experiment. Note that it is possible to set $\Delta E < 0$ and move the detector for seeing a signal with $E_{\mathrm{sig},I} < E_{\mathrm{opt}}$; however, a red shifted signal would be strongly attenuated by the filter.

The raw signal shown in the CCD image reported in Fig. 1(a) was obtained at $(\Delta T_{FF}, \Delta T_{FL}) = (0, 0)$, integrating over 3000 FEL shots. The spectrum of this signal is reported in Fig. 1(d). In addition to the expected inelastic FWM signal, we also observed a signal corresponding to $\Delta E = 0$ meV; the presence of such an "elastic" FWM signal may be caused by a residual spectral overlap (see Supplement 1). We note that these two signals have comparable intensities after the high pass filter. The bandwidth of both signals is of about 70 meV FWHM, which is of the same order of the combined bandwidth from the FEL (∼50 meV FWHM) and from the laser (∼10 meV FWHM). However, since the color filter has a strongly varying transmission between the elastic and inelastic peaks, the spectral shape of the observed signal can thus be different from the natural emission spectrum.

The set-up allows scanning both the relative delay between the two sequences of FEL pulses (ΔT_{FF}) and the delay between the optical pulse and the (E^B_{EUV1}; E^B_{EUV2}) pulse sequence (ΔT_{FL}). These two delay scans are independent from each other, with all ΔT_{FL} scans being performed at $\Delta T_{FF} = 0$ and all ΔT_{FF} scans being performed at $\Delta T_{FL} = 0$; see Refs. [21,22] for further details on the set-up.

The spectrum of the two-color FEL pulses and the variation of their intensity ratio during a ΔT_{FL} scan are shown, respectively, in Figs. 2(a) and 2(b). The former shows the FEL spectrum averaged over the $1.5 * 10^5$ FEL shots needed to collect a dataset, while the latter reports the intensity stability of the two colors (blue and red squares) and their ratio (green diamond). Data points in Fig. 2(b) were collected equally spaced in real time, and each one required 1 min of acquisition, corresponding to 3000 FEL shots (the FEL repetition rate was 50 Hz); the figure illustrates the high FEL stability in the tens of minutes scale.

3. RESULTS

Figure 3(a) reports a ΔT_{FF} scan, with both the elastic (red dots) and inelastic (black dots) signals well described by Gaussian shapes with $\sigma = 40 \pm 5$ fs. This is compatible with the cross-correlation of the FEL pulses, which is estimated to be about $\sigma \approx 30$ fs. We remind the reader that the latter is based on an estimate of the FEL pulse lengths [26,27], while the actual pulse length may have been longer.

ΔT_{FF} "photon echo" scans are sensitive to the ultrafast processes that yield the material excitation and their eventual dephasing [28]. In our case, the dominating process is photoionization, which happens on timescales shorter than our pulse duration [29,30]; one would therefore expect to observe merely a cross-correlation response without detectable dynamics.

The ΔT_{FL} scans reported in Fig. 3(b) instead display different dynamics for the two signals, and as evidenced by the solid purple Gaussian with $\sigma = 40$ fs, both differ from the ones reported in Fig. 3(a). The latter are much narrower in time since their width does not depend on the pulse duration and large wavefront tilt of the optical laser.

The elastic signal shown in Fig. 3(b) (red open dots) has an asymmetric temporal profile similar to the one observed in EUV-optical TG experiments. It can be modeled by a Gaussian rise with $\sigma_E = 104 \pm 5$ fs and an exponential decay with a decay time of 130 ± 10 fs plus a small offset at positive delays. The former is compatible with the FEL-laser cross-correlation, which sets the

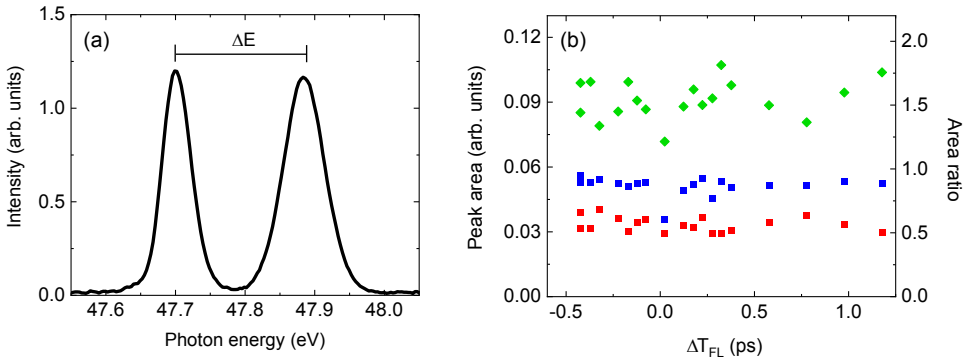

Fig. 2. (a) Average FEL spectrum over a ΔT_{FL} scan; the value of ΔE is indicated by the horizontal segment. (b) Peak area of the two FEL pulses (red and blue squares; left vertical scale) and their ratio (green diamonds; right vertical scale) during a time delay scan. Data are reported as a function of ΔT_{FL} but were collected equally spaced in real time, and each point represents the average over 3000 FEL shots. The stability of these values makes data normalization not critical.

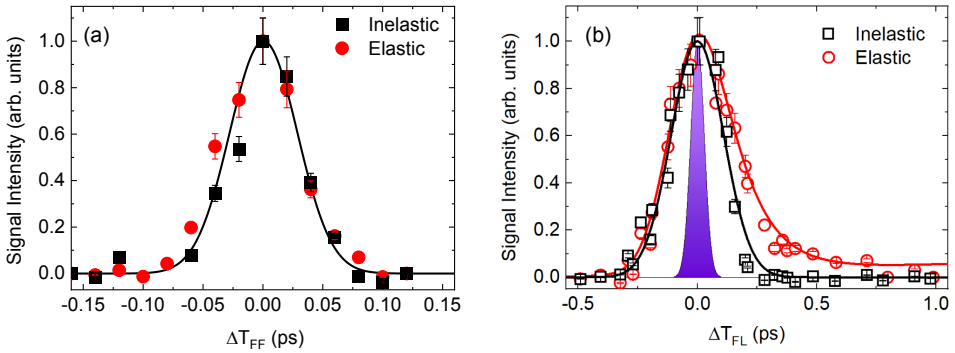

Fig. 3. (a) Experimental signals obtained by scanning ΔT_{FF}. Both the inelastic (full black squares) and elastic (full red dots) FWM signals show a Gaussian shape compatible with the cross-correlation between the two FEL pulses (black line). (b) The inelastic (open black squares) and elastic (open red dots) signals obtained by scanning ΔT_{FL} instead show different time dependencies. The latter is characterized by a Gaussian rise, compatible with the FEL-optical cross-correlation, and an exponential decay plus a small offset for $\Delta T_{FL} > 0$ (red line). The inelastic FWM signal has a narrower and more symmetric shape; the black line is a Gaussian function. The solid purple Gaussian is the FEL-FEL cross-correlation, i.e., the black line in (a).

time resolution of the experiment and is limited by the time duration of the optical pulse and the large wavefront tilt, once again indicating the impossibility to resolve the excitation mechanism with such long pulses. The decay time can be instead associated with the electron-lattice relaxation, which in carbon is typically hundreds of fs [31,32]. Such a relaxation of the population of the electronic excited states is the first step for driving the thermoelastic dynamics of the system [33,34], which can explain the small offset at positive delays. We refrain here from making a direct comparison with previous EUV-optical TG measurements conducted on diamond [34] for two reasons: 1) thanks to the filter, the set-up was optimized to collect the inelastic FWM signal, and the unexpected elastic signal was clearly observed only at FEL fluences much larger than those used in the EUV-optical TG; 2) the pre- and post-pulses were not present in previous EUV-optical TG measurements. Further measurements as a function of ΔE, including $\Delta E = 0$, possibly with controlled spectral overlap conditions, and in the presence of the pre- and post-pulse are required to assess the possible TG nature of the elastic FWM signal.

Conversely, the inelastic FWM signal [black open squares in Fig. 3(b)] has a narrower and more symmetric profile, reproduced here with a Gaussian of $\sigma_I = 110 \pm 5$ fs. This is compatible with the laser/FEL cross correlation, suggesting that we are essentially observing the instantaneous crystal polarization response (coherent spike) [35,36].

Data in Figs. 3(a) and 3(b) have been normalized by the sum of the squared values of the total FEL intensity, monitored shot-by-shot, in order to account for FEL fluctuations during the scans; the intensity of the optical laser was constant. The curves were then scaled to set their maxima to one for easier comparison. The normalization by the total FEL intensity squared rather than the product of the two FEL spectral lines is justified by the trends reported in Fig. 2(b), which show an essentially constant trend in the intensity ratio between the two spectral lines (green diamonds).

The dependence of the inelastic signal on the FEL intensity at $(\Delta T_{FF}, \Delta T_{FL}) = (0, 0)$ is shown in Fig. 4. The quadratic dependence (red solid line in Fig. 4) confirms that the observed inelastic signal has a FWM origin. The trend of the elastic signal is also compatible with a quadratic dependence; see Supplement 1 for further details.

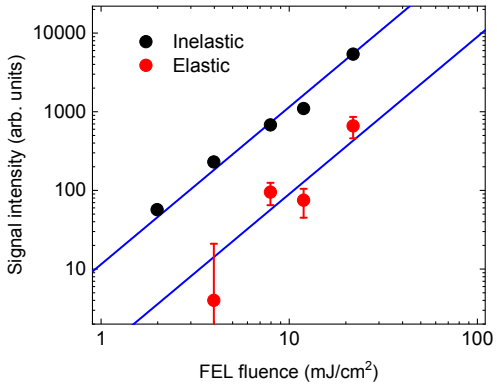

Fig. 4. Dependence of the inelastic (black circles) and elastic (red circles) FWM signal intensity at $(\Delta T_{FF}, \Delta T_{FL}) = (0, 0)$ on the FEL fluence. Fluence has been calculated as the energy of a single FEL pulse, divided by the spot area. Blue lines are quadratic fits to the data forced to pass for the origin of the Cartesian plane.

4. DISCUSSION

Having both the inelastic and elastic signals recorded simultaneously, the strength of the two processes can be straightforwardly compared. Following the estimate done in Ref. [13] and further considering the filter transmission, effective values of the third-order susceptibilities [1,37] can be estimated, namely, $\chi_I^{(3)} = 1.4 * 10^{-25}$ m^{2}V^{-2} and $\chi_E^{(3)} = 1.5 * 10^{-23}$ m^{2}V^{-2} for, respectively, the inelastic and elastic FWM signals; the $\chi_E^{(3)}$ estimate further assumes that the unexpected elastic FWM signal is proportional to the spectral overlap (see Supplement 1). At the lower investigated fluences, the signal level is close to the detection limit of the employed set-up. Much weaker FWM signals can be likely detected, for instance, by focusing the signal at the detector and better rejecting spurious light, to improve the S/N, or by exploiting EUV core–hole resonances to enhance the signal [8,17,18]; this potentially allows for single-shot data.

The observed frequency shift of the inelastic FWM signal indicates that it is related to the photon energy difference between the two FEL pulses. Diamond has an optical phonon at 165 meV [38,39], which, given the pulse bandwidth and the employed value of $\Delta E = 180$ meV, should fall within the possible range in photon energy difference of the employed FEL pulses and lead to a ps decay

in the inelastic signal, via a coherent anti-Stokes Raman scattering (CARS) mechanism [40,41]. However, we did not observe it, most likely because the pre-pulse causes a significant sample heating, which can substantially alter the phonon frequency and population; furthermore, the post-pulse would destroy any coherent population after 350 fs. The consistency of the time dependence of the inelastic FWM signal with the pulse cross-correlation [Fig. 3(b)] suggests that we are essentially observing a coherent spike, due to the "instantaneous" crystal polarization, i.e., the two-color FEL pulses drive the nonlinear polarization oscillating at $\Delta E/\hbar$, while the coupling with the probe field stimulates the emission of the inelastic FWM signal beam at $E_{\mathrm{opt}} + \Delta E$. In order to confirm this working hypothesis, further experiments as a function of ΔE could be performed. We expect the time dependence of the inelastic FWM signal to be independent from ΔE, while the signal emission angle should change according to the phase matching; see Fig. 1(c) and Supplement 1. Moreover, the heating due to the pre-pulse is not expected to play a significant role, since the instantaneous nonlinear polarization is weakly temperature dependent [1,37].

Additional FWM processes may contribute to both the inelastic and elastic signals. Their evaluation is beyond the scope of the present paper and are presently under detailed scrutiny, also with the aid of calculations, and will be presented in a separate paper [42]. However, it is evident how a significant step forward in this context would be to remove the additional (pre- and post-) pulses. This can be achieved by modifying the split–recombination set-up [21,22], for example, by replacing the splitting mirror with diffractive optics. In this way the different spectral components of the FEL emission can be spatially separated, and simple beam-blocks can prevent undesired pulses to reach the sample. The foreseeable drawbacks of this approach are the lower photon throughput and the need for realignment during ΔE scans; most likely both of them are not showstoppers.

5. CONCLUSIONS

We experimentally demonstrated an EUV-optical FWM process involving two EUV pulses with different photon energies. Despite the low repetition rate and without tuning the EUV photon energy to core resonances, we were able to observe a signal that is about 10^{10} times weaker than the probe pulse. This is due to the high S/N, which arises from spectral filtering and the phase-matching condition for noncollinear FWM processes. The results of the present work open the way towards putting into practice long theorized experiments, where ultrafast electronic dynamics and correlations between different atomic species can be studied [81]. The temporal resolution may be substantially improved using three noncollinear EUV pulses, which can be sub-fs, and diffractive set-ups [43]. This would also extend the range of ΔE into the multi-eV range, matching the energy of valence band excitations [8], while the exploitation of core resonances can provide chemical sensitivity. Multi-color FEL pulses with an energy separation of a few eV have already been demonstrated [44].

Inelastic EUV FWM can likely be performed also on metals and other probe-opaque samples, by using reflection geometry, which has already been used in TG experiments with optical probing [34]. Inelastic FWM permits to use spectral filtering, which is expected to strongly suppress elastic scattering by surface roughness, thus alleviating the sample surface quality requirements.

The described approach can also be extended to low density samples, such as atomic and molecular jets, where the excitation volume is not strongly limited by the penetration depth, but rather by the beam intersection, which can easily be some orders of magnitude larger than the penetration depth in condensed matter. This can compensate for the linear decrease of the signal strength due to the decrease in the density, since the FWM signal quadratically increases with the length of the interaction volume [45]. Moreover, solid-state samples are limited to relatively small FEL fluences by sample damage, while flowing samples are not, since in typical conditions they are "renewed" after each FEL shot. This would also enable studying FWM processes in a high field regime.

Funding. Schweizerischer Nationalfonds zur Förderung der Wissenschaftlichen Forschung (200021_165550/1); Office of Science (DE-SC0019126); Marie Skłodowska-Curie grant (860553).

Acknowledgment. We feel that it should become a good practice to inform the society about the energy cost of papers. Considering the energy needed to acquire the data and to analyze them, and the energy that was employed to allow collaborators to reach the FERMI facility, the paper costs about 368 MWh.

Disclosures. The authors declare no conflicts of interest.

Data availability. Data underlying the results presented in this paper are not publicly available at this time but may be obtained from the authors upon reasonable request.

Supplemental document. See Supplement 1 for supporting content.

REFERENCES

1. N. Bloembergen, "Nonlinear optics and spectroscopy," Rev. Mod. Phys. **54**, 685–695 (1982).
2. E. Cinquanta, D. Meggiolaro, S. G. Motti, M. Gandini, M. J. P. Alcocer, Q. A. Akkerman, C. Vozzi, L. Manna, F. De Angelis, A. Petrozza, and S. Stagira, "Ultrafast THz probe of photoinduced polarons in lead-halide perovskites," Phys. Rev. Lett. **122**, 166601 (2019).
3. M. Ossiander, M. L. Meretska, H. K. Hampel, S. W. D. Lim, N. Knefz, T. Jauk, F. Capasso, and M. Schultze, "Extreme ultraviolet metalens by vacuum guiding," Science **380**, 59–63 (2023).
4. S. Pirandola, U. L. Andersen, L. Banchi, M. Berta, D. Bunandar, R. Colbeck, D. Englund, T. Gehring, C. Lupo, C. Ottaviani, and J. L. Pereira, "Advances in quantum cryptography," Adv. Opt. Photon. **12**, 1012–1236 (2020).
5. E. Beaurepaire, J. C. Merle, A. Daunois, and J. Y. Bigot, "Ultrafast spin dynamics in ferromagnetic nickel," Phys. Rev. Lett. **76**, 4250–4253 (1996).
6. A. Vega-Flick, R. A. Duncan, J. K. Eliason, J. Cuffe, J. A. Johnson, J. P. M. Peraud, L. Zeng, Z. Lu, A. A. Maznev, E. N. Wang, and J. J. Alvarado-Gil, "Thermal transport in suspended silicon membranes measured by laser-induced transient gratings," AIP Adv. **72**, 235110 (2016).
7. C. Bacellar, D. Kinschel, G. F. Mancini, R. A. Ingle, J. Rouxel, O. Cannelli, C. Cirelli, G. Knopp, J. Szlachetko, F. A. Lima, and S. Menzi, "Heme doming in ferric cytochrome c: femtosecond X-ray absorption and X-ray emission studies," in *22nd International Conference on Ultrafast Phenomena*, Optica (2020), paper Th1A.2.
8. S. Tanaka and S. Mukamel, "Coherent X-Ray Raman spectroscopy: a nonlinear local probe for electronic excitations," Phys. Rev. Lett. **89**, 043001 (2002).
9. S. Mukamel, "Multiple core-hole coherence in x-ray four-wave-mixing spectroscopies," Phys Rev B. **72**, 235110 (2005).
10. S. Tanaka and S. Mukamel, "X-ray four-wave mixing in molecules," J. Chem. Phys. **116**, 1877–1891 (2022).
11. E. Sistrunk, J. Grilj, J. Jeong, M. G. Samant, A. X. Gray, H. A. Dürr, S. S. Parkin, and M. Gühr, "Broadband extreme ultraviolet probing of transient gratings in vanadium dioxide," Opt. Express **23**, 4340–4347 (2015).
12. F. Bencivenga, R. Mincigrucci, F. Capotondi, L. Foglia, D. Naumenko, A. A. Maznev, E. Pedersoli, A. Simoncig, F. Caporaletti, V. Chiloyan, and R. Cucini, "Nanoscale transient gratings excited and probed by extreme ultraviolet femtosecond pulses," Sci. Adv. **5**, eaaw5805 (2019).

13. F. Bencivenga, R. Cucini, F. Capotondi, A. Battistoni, R. Mincigrucci, E. Giangrisostomi, A. Gessini, M. Manfredda, I. P. Nikolov, E. Pedersoli, and E. Principi, "Four-wave mixing experiments with extreme ultraviolet transient gratings," Nature **520**, 205–208 (2015).
14. J. R. Rouxel, D. Fainozzi, R. Mankowsky, B. Rösner, G. Seniutinas, R. Mincigrucci, S. Catalini, L. Foglia, R. Cucini, F. Döring, and A. Kubec, "Hard X-ray transient grating spectroscopy on bismuth germanate," Nat. Photonics **15**, 499–503 (2021).
15. R. K. Lam, S. L. Raj, T. A. Pascal, C. D. Pemmaraju, L. Foglia, A. Simoncig, N. Fabris, P. Miotti, C. J. Hull, A. M. Rizzuto, and J. W. Smith, "Soft X-ray second harmonic generation as an interfacial probe," Phys. Rev. Lett. **120**, 023901 (2018).
16. S. Shwartz, M. Fuchs, J. B. Hastings, Y. Inubushi, T. Ishikawa, T. Katayama, D. A. Reis, T. Sato, K. Tono, M. Yabashi, and S. Yudovich, "X-ray second harmonic generation," Phys. Rev. Lett. **112**, 163901 (2014).
17. H. Rottke, R. Y. Engel, D. Schick, J. O. Schunck, P. S. Miedema, M. C. Borchert, M. Kuhlmann, N. Ekanayake, S. Dziarzhytski, G. Brenner, and U. Eichmann, "Probing electron and hole colocalization by resonant four-wave mixing spectroscopy in the extreme ultraviolet," Sci. Adv. **8**, eabn5127 (2022).
18. F. Bencivenga, S. Baroni, C. Carbone, M. Chergui, M. B. Danailov, G. De Ninno, M. Kiskinova, L. Raimondi, C. Svetina, and C. Masciovecchio, "Nanoscale dynamics by short-wavelength four wave mixing experiments," New J. Phys. **15**, 123023 (2013).
19. Y. Zhang, D. Healion, J. D. Biggs, and S. Mukamel, "Double-core excitations in formamide can be probed by X-ray double-quantum-coherence spectroscopy," J. Chem. Phys. **138**, 144301 (2013).
20. S. Mukamel, D. Healion, Y. Zhang, and J. D. Biggs, "Multidimensional attosecond resonant X-ray spectroscopy of molecules: lessons from the optical regime," Annu. Rev. Phys. Chem. **64**, 101–127 (2013).
21. R. Mincigrucci, L. Foglia, D. Naumenko, E. Pedersoli, A. Simoncig, R. Cucini, A. Gessini, M. Kiskinova, G. Kurdi, N. Mahne, and M. Manfredda, "Advances in instrumentation for FEL-based four-wave-mixing experiments," Nucl. Instrum. Methods Phys. Res. A **907**, 132–148 (2018).
22. F. Bencivenga, R. Mincigrucci, F. Capotondi, A. Calvi, R. Cucini, L. Foglia, E. Pedersoli, E. Principi, A. Simoncig, P. Cinquegrana, and M. B. Danailov, "An approach for realizing four-wave-mixing experiments stimulated by two-color extreme ultraviolet pulses," Proc. SPIE **11886**, 118860E (2021).
23. F. Trojánek, K. Žídek, B. Dzurňák, M. Kozák, and P. Malý, "Nonlinear optical properties of nanocrystalline diamond," Opt. Express **18**, 1349–1357 (2010).
24. V. I. Gavrilenko and F. Rebentrost, "Nonlinear optical susceptibility of the surfaces of silicon and diamond," Surf. Sci. **331-333**, 1355–1360 (1995).
25. S. Reilly, V. G. Savitski, H. Liu, S. Reid, D. Gibson, H. Dhillon, S. O. Robbie, E. Gu, M. D. Dawson, A. Bennett, and A. J. Kemp, "Laser induced damage threshold of CVD-grown single crystal diamond surfaces with various surface finishes," in *Advanced Solid State Lasers* (Optica, 2015), paper ATu2A.6.
26. D. Ratner, A. Fry, G. Stupakov, and W. White, "Laser phase errors in seeded free electron lasers," Phys. Rev. Spec. Top. Accel. Beams. **15**, 030702 (2012).
27. P. Finetti, H. Höppner, E. Allaria, C. Callegari, F. Capotondi, P. Cinquegrana, M. Coreno, R. Cucini, M. B. Danailov, A. Demidovich, and G. De Ninno, "Pulse duration of seeded free-electron lasers," Phys Rev X. **7**, 021043 (2017).
28. I. D. Abella, N. A. Kurnit, and S. R. Hartmann, "Photon echoes," Phys. Rev. **141**, 391–406 (1966).
29. W. K. Peters, T. Jones, A. Efimov, E. Pedersoli, L. Foglia, R. Mincigrucci, I. Nikolov, R. Trebino, M. B. Danailov, F. Capotondi, and F. Bencivenga, "All-optical single-shot complete electric field measurement of extreme ultraviolet free electron laser pulses," Optica **8**, 545–550 (2021).
30. R. Bohinc, G. Pamfilidis, J. Rehault, P. Radi, C. Milne, J. Szlachetko, F. Bencivenga, F. Capotondi, R. Cucini, L. Foglia, and C. Masciovecchio, "Nonlinear XUV-optical transient grating spectroscopy at the Si $L_{2,3}$ –edge," Appl. Phys. Lett. **114**, 181101 (2019).
31. R. Mincigrucci, E. Principi, F. Bencivenga, L. Foglia, A. Gessini, G. Kurdi, A. Simoncig, and C. Masciovecchio, "Transient EUV reflectivity measurements of carbon upon ultrafast laser heating," Photonics **4**, 23 (2017).
32. E. Principi, S. Krylow, M. E. Garcia, A. Simoncig, L. Foglia, R. Mincigrucci, G. Kurdi, A. Gessini, F. Bencivenga, A. Giglia, and S. Nannarone, "Atomic and electronic structure of solid-density liquid carbon," Phys. Rev. Lett. **125**, 155703 (2020).
33. F. Bencivenga, F. Capotondi, L. Foglia, R. Mincigrucci, and C. Masciovecchio, "Extreme ultraviolet transient gratings," Adv Phys. X **8**, 2220363 (2023).
34. A. A. Maznev, F. Bencivenga, A. Cannizzo, F. Capotondi, R. Cucini, R. A. Duncan, T. Feurer, T. D. Frazer, L. Foglia, H. M. Frey, and H. Kapteyn, "Generation of coherent phonons by coherent extreme ultraviolet radiation in a transient grating experiment," Appl. Phys. Lett. **113**, 221905 (2018).
35. M. V. Lebedev, O. V. Misochko, T. Dekorsy, and N. Georgiev, "On the nature of "coherent artifact"," J. Exp. Theor. Phys. **100**, 272–282 (2005).
36. M. W. Balk and G. R. Fleming, "Dependence of the coherence spike on the material dephasing time in pump–probe experiments," J. Chem. Phys. **83**, 4300–4307 (1985).
37. S. Mukamel, *Principles of Nonlinear Optical Spectroscopy*, Oxford Series in Optical and Imaging Sciences (Oxford University, 1995), p. 543.
38. I. Pope, L. Payne, G. Zoriniants, E. Thomas, O. Williams, P. Watson, W. Langbein, and P. Borri, "Coherent anti-Stokes Raman scattering microscopy of single nanodiamonds," Nat. Nanotechnol. **9**, 940–946 (2014).
39. S. A. Solin and A. K. Ramdas, "Raman spectrum of diamond," Phys. Rev. B **1**, 1687–1698 (1970).
40. A. Laubereau and W. Kaiser, "Vibrational dynamics of liquids and solids investigated by picosecond light pulses," Rev. Mod. Phys. **50**, 607–665 (1978).
41. A. Laubereau, D. Von Der Linde, and W. Kaiser, "Direct measurement of the vibrational lifetimes of molecules in liquids," Phys. Rev. Lett. **28**, 1162–1165 (1972).
42. G. Pamfilidis, F. Bencivenga, P. Radi, *et al.* are preparing a manuscript to be called "Mixed XUV/Optical coherent four wave mixing scattering using a free electron laser."
43. M. Krstulovic, H.-Y. Chen, R. Mincigrucci, *et al.* are preparing a manuscript to be called "Coherent multi-eV excitation of MgO exciton."
44. E. Ferrari, C. Spezzani, F. Fortuna, R. Delaunay, F. Vidal, I. Nikolov, P. Cinquegrana, B. Diviacco, D. Gauthier, G. Penco, and P. R. Ribič, "Widely tunable two-colour seeded free-electron laser source for resonant-pump resonant-probe magnetic scattering," Nat. Commun. **7**, 10343 (2016).
45. L. Foglia, R. Mincigrucci, A. A. Maznev, G. Baldi, F. Capotondi, F. Caporaletti, R. Comin, D. De Angelis, R. A. Duncan, D. Fainozzi, and G. Kurdi, "Extreme ultraviolet transient gratings: a tool for nanoscale photoacoustics," Photoacoustics **29**, 100453 (2023).